Progress In Electromagnetics Research M, Vol. 113, 129–138, 2022

A Series-Series Compensated Contactless Power Transfer Based on the Rotary Transformer for the Drilling System

Ruiwen Kong[1] and Liuge Du[2, *]

Abstract—The electrical representation of the contactless power transfer (CPT) system with a coaxial transformer for the power traction in the rotary drilling system is presented. The air gap in the rotary transformer can lead to a lot of leakage inductance, so that the series-series (SS) compensation capacitors are used to increase the efficiency and the capability of the system. Moreover, the frequency response of the SS compensated CPT system is analyzed, and the transfer characteristics of the CPT system are revealed at different resonant frequencies. It is shown that the phase angle of the input impedance at resonant frequency determines the operation mode of the CPT system. At resonant frequency ω_0, the system can operate in constant-current (CC) mode, whereas at resonant frequency ω_H, it can work in constant-voltage (CV) mode. In the application of the drilling system, the CV mode owning good load regulation is more preferred than the CC mode for a wide range of load variation. At last, the analysis result is verified by experiment. The experimental results indicate that the CPT system in the CV mode can produce a $30 \sim 35$ V voltage output and can transfer maximum power 180 W with an efficiency of 78.5%. The proposed CPT system can well meet the requirement of power supply in the drilling system.

1. INTRODUCTION

In some mechatronic systems, the transfer of power from a stationary to a rotating structure, which involves wearable parts such as slip rings, plays an important role in robotics and rotating electronics. Despite the development of a reliable and durable slip ring, its lifetime is still limited by contact wear, vibration, and high temperature. As a result, frequent maintenance or even full replacement is required. A solution to overcome the disadvantages of slip rings is a contactless power transfer (CPT) system. The CPT using inductive coupling without a mechanical contact has the advantages of electrical isolation, safety, reliability, and low maintenance. The CPT technology has been used in various applications such as portable electronics [1], biomedical implants [2–4], battery charging [5–7], underwater devices [8], and solar wing driving [9], where physical connections are either inconvenient or dangerous. For the larger power transmission in a rotary electrical system, the CPT system with a rotating transformer is one of the good candidates [10, 11], which can output a continuous high power wirelessly. The rotary transformer is a loosely winding transformer with separated primary and secondary windings. Since the two windings of the transformer are physically separated by an air gap, the air gap can lead to a low coupling efficient and high leakage inductance, which results in poor power conversion. In order to minimize converter switching losses and to compensate for the high leakage inductance of the transformer, the compensation capacitors are used in CPT applications [12, 13].

In this paper, the electrical representation of a series-series (SS) compensated CPT system with air gap for the power traction in rotary drilling system is presented. The frequency response of the CPT system is analyzed, and the transfer characteristics of the CPT system are revealed at resonant frequencies. Furthermore, the analysis result is verified by experiment.

Received 2 July 2022, Accepted 7 September 2022, Scheduled 17 September 2022

* Corresponding author: Liuge Du (lgdu@sdu.edu.cn).

[1] School of Science and Engineering, The Chinese University of Hong Kong, Shenzhen 518172, China. [2] School of Information Science and Engineering, Shandong University, Qingdao 266237, China.

2. BASIC PRINCIPLE

The block diagram of the CPT system with a rotary transformer is demonstrated in Fig. 1. It can be seen that the whole system is mainly composed of power inverter, rotary transformer, full-bridge rectifier, capacitive filter, and load resistance. Generally, to improve the power transfer characteristics, a high-frequency resonant converter is adopted at the primary side. The rectifier/filter circuit in the secondary side is used to convert the high-frequency voltage to DC to supply the load.

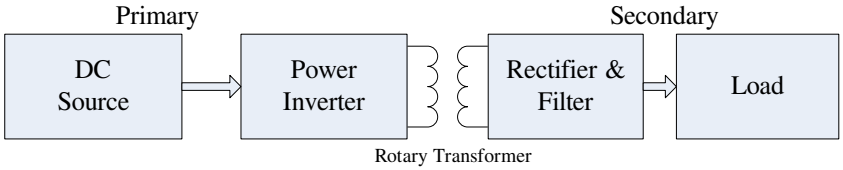

Figure 1. The block diagram of CPT system for rotary applications.

The rotary transformer is the key component of the CPT system. The coaxial structure of the rotary transformer is shown in Fig. 2. From Fig. 2, it can be clearly seen that air gap is provided between the primary and secondary windings making them entirely non-contact with each other, so that the secondary side can freely rotate relative to the primary side and the drilling shaft. The MnZn ferrite material is used to support the windings and enhance the magnetic coupling between the primary and secondary windings.

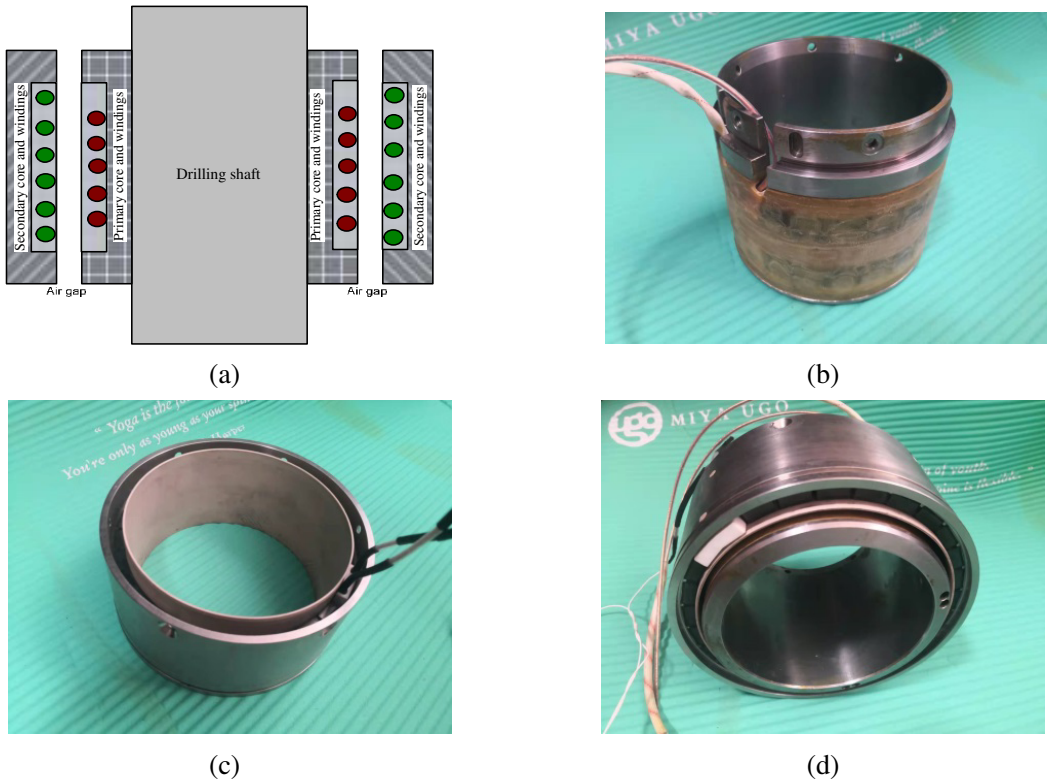

Figure 2. Schematic diagram and fabricated prototype of rotary transformer structures. (a) Schematic diagram. (b) Primary side. (c) Secondary side. (d) Combination of primary and secondary sides.

3. CIRCUIT CHARACTERISTICS

The CPT system with a rotary transformer is a loosely coupled inductive power transfer system and is characterized by missing the ferrite cores and having an air gap between the windings. Such a design results in a relatively large leakage inductance and low coupling coefficient. For this reason, in order to compensate the leakage on the inductances and improve the power transfer capability, the resonant capacitors at the primary and secondary windings are employed in CPT systems. Among the various compensation topologies, the SS topology has the advantage that the resonant frequency is independent of the load [14]. The configuration of the SS compensated CPT system is shown in Fig. 3. The rotary transformer with air gap is usually modeled by a coupled-inductor model. The compensation capacitors C_1 and C_2 are used in both the primary and secondary windings to increase the efficiency and the capability of the system.

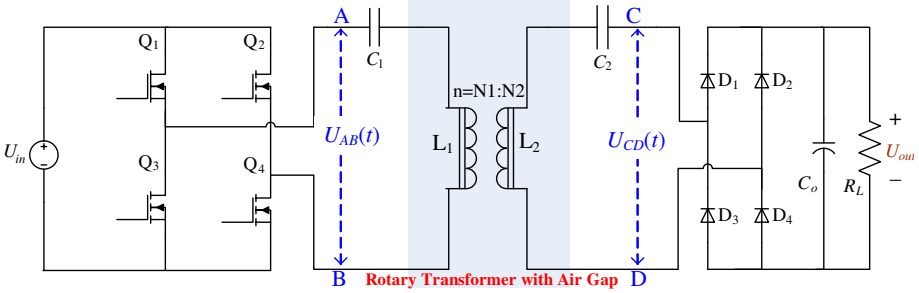

Figure 3. Configuration of the SS compensated CPT system.

An equivalent electrical representation of the CPT system is shown in Fig. 4. Since the fundamental harmonic of the square wave $V_{AB}(t)$ at the input is considered, the full-bridge rectifier, capacitive filter, and load resistance can be modeled by AC load resistance R_{Le} ($R_{Le} = 8R_L/\pi^2$) [15], as shown in Fig. 4(a). In addition, the winding resistance (R_1, R_2), the leakage inductances (L_{lk1}, L_{lk2}), the magnetizing inductance (L_m), the magnetic core loss (R_m), and the turns ratio of windings (N_1/N_2) are used to model the rotary transformer.

The equations for magnetizing inductance (L_m), leakage inductance (L_{lk1}, L_{lk2}), self-inductance (L_1, L_2), mutual-inductance (M), and coupling coefficient (k) are respectively denoted as

$$\begin{cases} L_1 = L_{lk1} + L_m \\ L_2 = L_{lk2} + L_m/n^2 \\ L_m = nM \\ k = \dfrac{M}{\sqrt{L_1 L_2}} \end{cases} \tag{1}$$

where the turns radio of windings is $n = N_1/N_2$.

In Eq. (1), the mutual inductance (M) and self-inductances (L_1, L_2) of the rotary transformer can be measured by using an impedance analyzer (LCR meter). The associated primary and secondary leakage inductances can be determined by the equations above.

To analyze the equivalent circuit of the CPT system effectively, the components in the secondary side of the ideal transformer are transformed to their equivalents in the primary side, as shown in Fig. 4(b). From Kirchhoff's voltage law, the input-to-output voltage gain can be obtained as follows [16]

$$G_V = \left|\frac{U_{out}}{U_{in}}\right| = \left|\frac{\frac{2\sqrt{2}}{\pi}U_{CD}}{\frac{2\sqrt{2}}{\pi}U_{AB}}\right| = \left|\frac{nZ_m R_{Le}}{\mathrm{n}^2(Z_1+Z_m)(Z_2+R_{Le})+Z_1 Z_m}\right| \tag{2}$$

where U_{AB} and U_{CD} indicate the fundamental components of $U_{AB}(t)$ and $U_{CD}(t)$ respectively. $Z_i = \mathrm{j}\omega L_{lki} + \frac{1}{\mathrm{j}\omega C_i} + R_i (i = 1, 2)$, $Z_m = \frac{\mathrm{j}\omega L_m R_m}{\mathrm{j}\omega L_m + R_m}$.

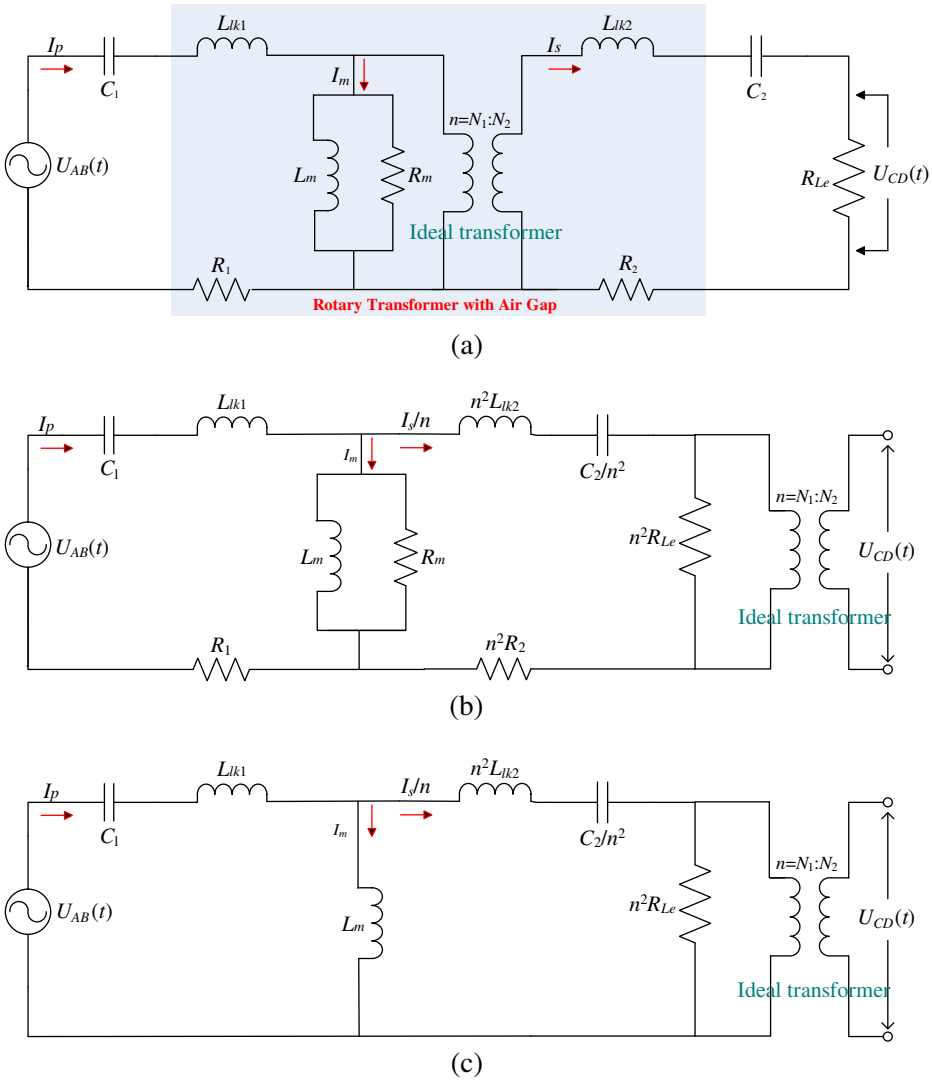

Figure 4. Equivalent electrical representation of the SS compensated CPT system. (a) Equivalent circuit. (b) Equivalent circuit in which the components in the secondary side of the ideal transformer are transformed to their equivalents in the primary side. (c) Equivalent circuit in which the winding resistances and the magnetic core loss are neglected.

If the winding resistances and the magnetic core loss are neglected, as shown in Fig. 4(c), Eq. (2) can be rewritten as

$$G_V = \left| \frac{n\omega L_m R_{Le}}{\mathrm{n}^2 Z_p (Z_s + R_{Le}) + (\omega L_m)^2} \right| = \left| \frac{\omega M R_{Le}}{Z_p (Z_s + R_{Le}) + (\omega M)^2} \right| \tag{3}$$

where $Z_p = \mathrm{j}\omega L_1 + \frac{1}{\mathrm{j}\omega C_1}$, $Z_s = \mathrm{j}\omega L_2 + \frac{1}{\mathrm{j}\omega C_2}$.

If the operating frequency is adjusted to the natural resonance frequency of the coil circuit, which is $\omega_0 = 1/\sqrt{L_1 C_1} = 1/\sqrt{L_2 C_2}$, the voltage gain can be simplified as

$$G_V = \frac{R_{Le}}{\omega_0 M} \tag{4}$$

When operating at the resonance frequency ω_0, G_V is in proportion to R_L, and the SS topology has a current-source characteristic.

If the compensation capacitors are selected randomly, Eq. (3) can be expressed as

$$G_V = \frac{1}{\left|\frac{Z_p}{\omega M} + \frac{\delta}{\omega^3 C_1 C_2 R_{Le} M}\right|} \tag{5}$$

where $\delta = \omega^4 C_1 C_2 L_1 L_2 (k^2 - 1) + \omega^2 (L_1 C_1 + L_2 C_2) - 1$.

Solving for roots of $\delta = 0$, two resonant frequencies at which G_V is load-independent can be obtained

$$\omega_L = \sqrt{\frac{\omega_p^2 + \omega_s^2 - \alpha}{2\left(1 - k^2\right)}} \quad \omega_H = \sqrt{\frac{\omega_p^2 + \omega_s^2 + \alpha}{2(1 - k^2)}} \tag{6}$$

where $\omega_p = \frac{1}{\sqrt{L_1 C_1}}$, $\omega_s = \frac{1}{\sqrt{L_2 C_2}}$, $\alpha = \sqrt{\left(\omega_p^2 + \omega_s^2\right)^2 - 4\left(1 - k^2\right)\left(\omega_p^2 + \omega_s^2\right)}$.

When operating at the resonance frequencies ω_L and ω_H, G_V satisfies the relationship of $G_V = |\omega M / Z_p|$, which means that G_V is independent of R_L, and the SS topology has a voltage-source characteristic. If the two leakage inductances are compensated using capacitances satisfying $\omega_p = \omega_s = \omega_0$, Eq. (6) can be simplified as

$$\omega_L = \frac{\omega_0}{\sqrt{1 + k}} \quad \omega_H = \frac{\omega_0}{\sqrt{1 - k}} \tag{7}$$

The input impedance Z_{in} as seen from by the source is given by

$$Z_{in} = Z_1 + \frac{n^2 \left(Z_2 + R_{Le}\right) Z_m}{n^2 \left(Z_2 + R_{Le}\right) + Z_m} = Z_1 + Z_m - \frac{Z_m^2}{n^2 \left(Z_2 + R_{Le}\right) + Z_m} \tag{8}$$

If the winding resistances and the magnetic core loss are neglected, Eq. (8) can be further expressed as

$$Z_{in} = Z_p + \frac{\omega^2 M^2}{Z_s + R_{Le}} = \frac{Z_p R_{Le}}{Z_s + R_{Le}} + \frac{\delta}{\omega^2 C_1 C_2 (Z_s + R_{Le})} \tag{9}$$

In order to attain high efficiencies of power transfer through CPT, the behavior of CPT efficiency with respect to the operating frequency of the power source should be concerned. The efficiency of power transfer from the source to the load is given by

$$\eta = \frac{P_L}{P_{in}} = \frac{|I_s|^2 R_{Le}}{|I_p|^2 \operatorname{Re}(Z_{in})} \tag{10}$$

where $\operatorname{Re}(Z_{in})$ is the real part of the input impedance.

From Fig. 4(b), $|I_p|/|I_s| = \frac{1}{n}\left|\frac{n^2(Z_2 + R_{Le})}{Z_m} + 1\right|$, the efficiency of power transfer can be rewritten as

$$\eta = \frac{n^2 R_{Le}}{\operatorname{Re}\left(Z_{in}\right)\left|\frac{n^2(R_{Le} + Z_2)}{Z_m} + 1\right|^2} \tag{11}$$

Equation (11) confirms that reducing the loss of winding coils, increasing mutual inductance between the primary and secondary windings, combined with the appropriate compensating network, can improve the efficiency of power transfer of the CPT system.

4. FREQUENCY RESPONSES ANALYSIS

The measured electric parameters of the CPT system are listed in Table 1. By using those parameters, the frequency responses of the input impedance,voltage gain, and power efficiency are calculated in detail, as shown in Fig. 5 and Fig. 6. The calculated results do not consider the switching loss at the primary side and the rectifier's energy loss at the secondary side. From Fig. 5, it can be observed that the input impedances at resonant frequency ω_L, ω_0, and ω_H are capacitive, resistive, and inductive

Table 1. Electronic parameters of the CPT system.

Parameter	Description	Value	Unit
L_1	Primary self-inductance	41.90	uH
L_2	Secondary self-inductance	66.25	uH
M	Mutual inductance	46.30	uH
k	Coupling coefficient	0.879	
n	Turn ratio of windings	5 : 6	
L_m	Magnetizing inductance	38.58	uH
L_{lk1}	Primary leakage inductance	3.32	uH
L_{lk2}	Secondary leakage inductance	10.69	uH
C_1	Primary compensation capacitor	330	nF
C_2	Secondary compensation capacitor	220	nF
R_1	Primary winding resistance	0.30	Ω
R_2	Secondary winding resistance	0.35	Ω
f	Operating frequency	30, 42, 120	kHz
V_{in}	Input DC voltage	32	V
R_L	Load resistance	5–40	Ω

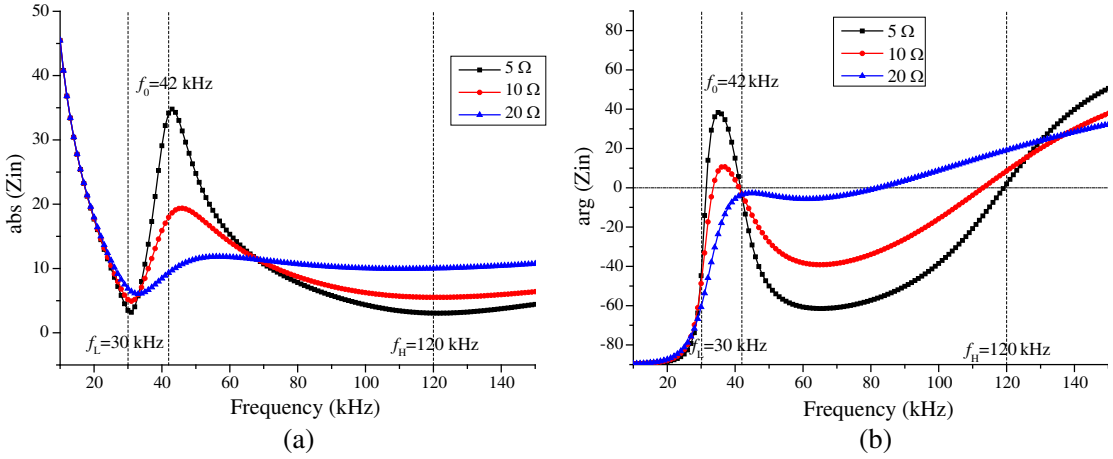

Figure 5. Calculated frequency response of input impedance as seen from the source. (a) Modulus of input impedance. (b) Phase of input impedance.

respectively. From Fig. 6, the power efficiency of the system increases with the frequency, and reaches a peak value at resonant frequency ω_0, then drops as the frequency extends.

Since the equivalent circuit at the first resonant frequency ω_0 consists of only a resister, the zero phase angles (ZPA) condition can be achieved, so that the input current is in phase with the input voltage. As a result, the input impedance is inversely proportion to load resistance, which makes the input current increase at the lighter load due to the low input impedance. This means that the SS topology can be operated in constant-current (CC) mode, which is not suitable for transferring power with large load variation.

At the resonant frequency ω_L, the input impedance is capacitive, and the current through the resonant circuit leads the input voltage. Thus, all switches in the inverter can be turned off with zero-current-switching (ZCS). However, the large angle of input impedance will reduce the voltage gain and

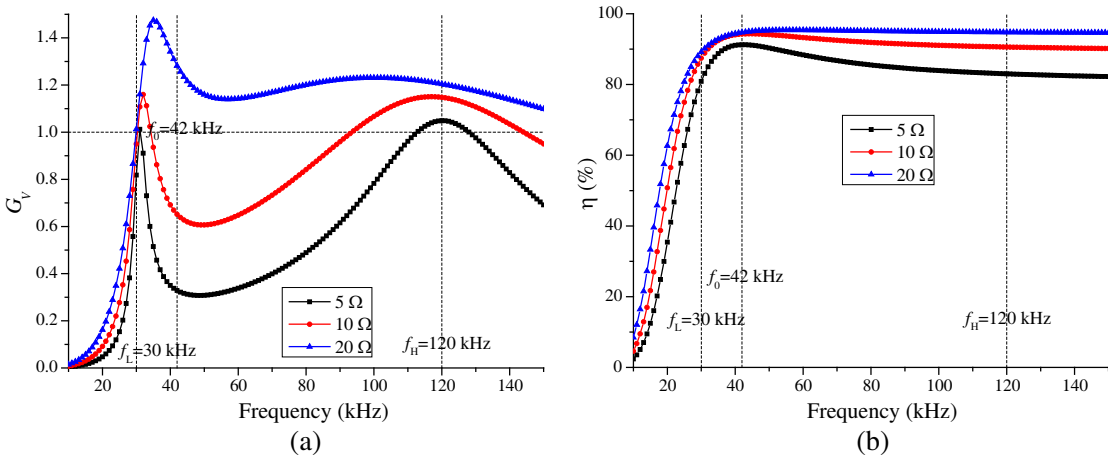

Figure 6. Calculated frequency responses of voltage gain and power efficiency. (a) Voltage gain. (b) Power efficiency.

efficiency of power transfer. Moreover, from Eq. (11), the efficiency power transfer cannot attain a higher level due to the lower resonant frequency, just as shown in Fig. 6. Therefore, the CPT system should avoid operating in this resonant frequency.

At the resonant frequency ω_H, the input impedance is inductive, and the input current lags the input voltage by the phase difference. As a result, all switches in the inverter can be turned on with zero-voltage-switching (ZVS). Thus, unlike the input impedance at the resonant frequencies ω_0, the input current decreases at the lighter load and the SS topology can give a constant-voltage (CV) output. It is worth noting that the input impedance at the resonant frequency ω_H is in proportion to the load resistance and that the ZPA condition can be achieved at a heavier load.

5. EXPERIMENTAL EVALUATION

Based on the analysis above, a prototype of the CPT system with a rotary transformer, as shown in Fig. 7, is built to verify the validity of the proposed design method. Relevant parameters of the prototype are shown in Table 1. The power supply side, fed by a 32 V DC source, is controlled by the full-bridge inverter to obtain a high-frequency AC voltage that go through the series compensation

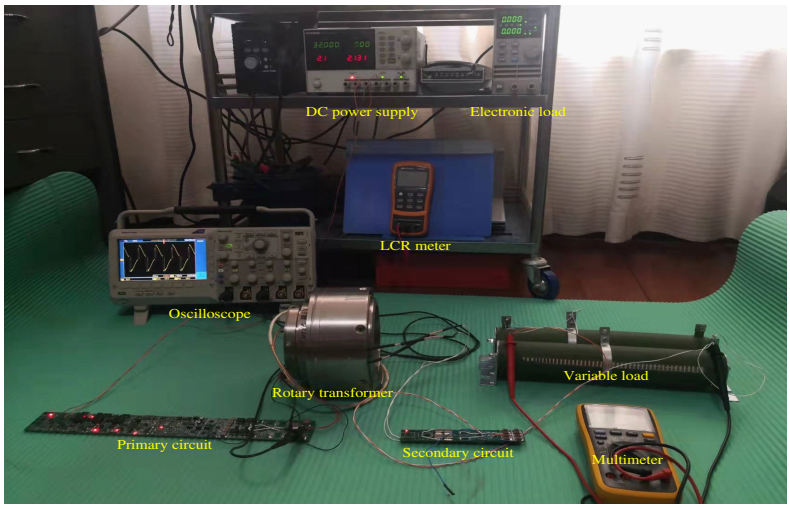

Figure 7. Experimental setup of the proposed CPT system.

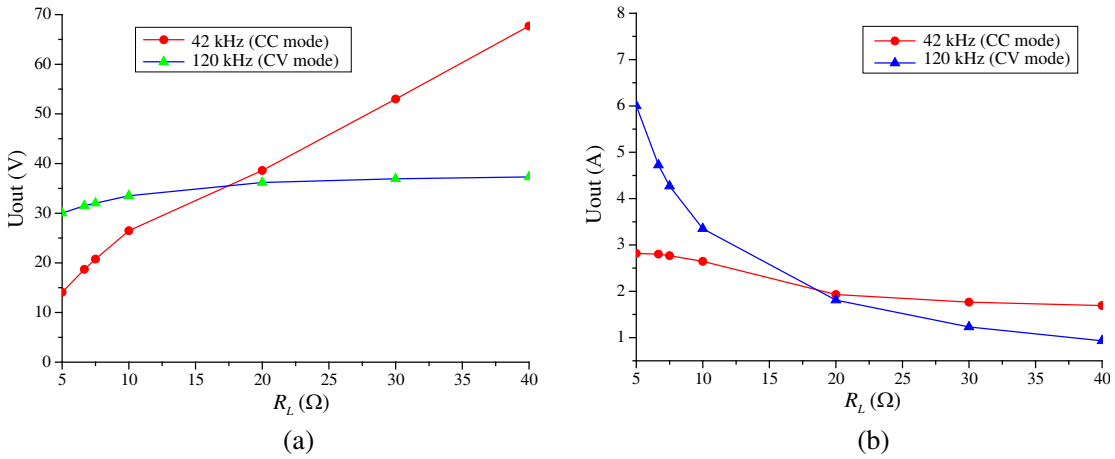

Figure 8. Measured output voltage and current under variable load at different resonance frequency. (a) Output voltage. (b) Output current.

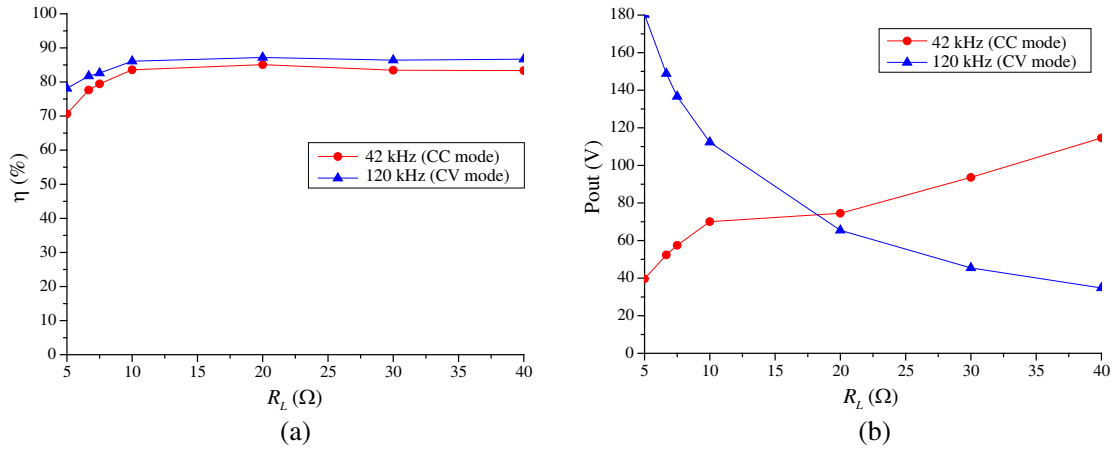

Figure 9. Measured output power and efficiency under variable load at different resonance frequency. (a) Efficiency of power transfer. (b) Output power.

circuit, while the secondary coil is connected to a full-bridge rectifier directly, and then an electronic load is connected to the rectifier. The output voltage, current, power, and efficiency are measured with the variation of output load at the two resonant frequencies (42 kHz, and 120 kHz), and the results are given in Fig. 8 and Fig. 9. The resonant frequency at 30 kHz is not discussed here due to its low efficiency in power transfer.

The experimental results indicate that the CPT system at the resonant frequency ω_0 works in CC mode, and the output current remains almost constant despite changes in light load resistance while it slightly increases at the heavy load resistance. In the experiment, the CPT system can transfer $2 \sim 3$ A current with an energy transfer efficiency of 82%.

At the resonant frequency ω_H, the CPT system operates in CV mode, and the output voltage is almost constant against load variation. However, it slightly decreases at the range of low load resistance. In the experiment, the CPT system in the CV mode can give a $30 \sim 35$ V voltage output and can transfer the maximum power about 180 W with an energy transfer efficiency of 78.5%. In case of the output power is less than 112 W, the transmission efficiency can reach above 86%. In rotary steering drilling system, the maximum power output of the CPT system is about 100 W. The proposed CPT system can well meet the requirement of power supply in the drilling system.

Whether the CPT system works in CC mode or CV mode, the load-independent theory is

established under the assumption of ignorable parasitic resistances, which is no longer applicable when the load resistance becomes smaller. As a result, the ideal CV and CC modes cannot be achieved at the smaller load resistance.

6. CONCLUSION

The electrical representation of the SS compensated CPT system for the power traction in rotary drilling system is presented. The frequency response of the CPT system is analyzed, and the transfer characteristics of the CPT system are illustrated at three resonant frequencies: one resonant frequency determined by self-inductance and compensation capacitor and the other two resonant frequencies determined by leakage inductance,mutual inductance, and compensation capacitor. The input impedance analysis shows that the phase of input impedance at resonant frequencies determines the operation mode of the CPT system. At resonant frequencies ω_0, it can operate in CC mode, while at resonant frequencies ω_H, it can operate in CV mode. Superior to the CC mode, the CV mode is more preferred in the application of the drilling system for a wide range of load variations because of the characteristic of good load regulation. At last, the analysis results are verified experimentally. The experimental results indicate that the CPT system in the CV mode can give a $30 \sim 35$ V voltage output and can transfer the maximum power 180 W with an efficiency of 78.5%, which can well meet the requirement of power supply in the drilling system.

REFERENCES

1. Park, J. Y., C. J. Park, and Y. J. Shin, "Planar multiresonance reactive shield for reducing electromagnetic interference in portable wireless power charging application," *Appl. Phys. Lett.*, Vol.114, 203902, 2019.
2. Chen, Q., S. C. Wong, and C. K. Tse, "Analysis, design, and control of a transcutaneous power regulator for artificial hearts," *IEEE Trans. Biomed. Circuits Syst.*, Vol. 3, No. 1, 23–31, 2009.
3. Mohammad, H. and S. Reem, "Wireless power transfer approaches for medical implants: A review," *Signals*, No. 1, 209–229, 2020.
4. Agarwal, K., R. Jegadeesan, and Y. X. Guo, "Wireless power transfer strategies for implantable bioelectronics," *IEEE Rev. Biomed. Eng.*, Vol. 10, 136–161, 2017.
5. Jung, S., H. Lee, and C. S. Song, "Optimal operation plan of the online electric vehicle system through establishment of a DC distribution system," *IEEE Trans. Power Electron.*, Vol. 28, No. 12, 5878–5889, 2013.
6. Ali, Z., V. Z. Sadegh, and B. Amir, "A dynamic WPT system with high efficiency and high power factor for electric vehicles," *IEEE Trans. Power Electron.*, Vol. 35, No. 7, 6732–6740, 2020.
7. Kadem, K., F. Benyoubi, M. Bensetti, Y. L. Bihan, E. Labouré, and M. Debbou, "An efficient method for dimensioning magnetic shielding for an induction electric vehicle charging system," *Progress In Electromagnetics Research*, Vol. 170, 153–167, 2021.
8. Yan, Z. C., B. W. Song, and Y. M. Zhang, "A rotation-free wireless power transfer system with stable output power and efficiency for autonomous underwater vehicles," *IEEE Trans. Power Electron.*, Vol. 34, No. 5, 4005–4008, 2019.
9. Song, K., B. Q. Ma, and G. Yang, "A rotation-light weight wireless power transfer system for solar wing driving," *IEEE Trans. Power Electron.*, Vol. 34, No. 9, 8816–8830, 2019.
10. Papastergiou, K. D. and D. E. Macpherson, "An airborne radar power supply with contactless transfer of energy-part I: Rotating transformer," *IEEE Trans. Ind. Electron.*, Vol. 54, No. 5, 2874–2884, 2007.
11. Moradewicz, A., "Contactless energy transmission system with rotatable transformer-modeling, analyzes and design," Ph.D. Dissertation, Electrotechnical Institute, Warsaw, Poland, 2008.
12. Zhang, W. and C. C. Mi, "Compensation topologies of high-Power wireless power transfer systems," *IEEE Trans. Veh. Technol.*, Vol. 65, No. 6, 4768–4778, 2016.

13. Zhang, W., S. Wong, and C. K. Tse, "Design for efficiency optimization and voltage controllability of series-series compensated inductive power transfer systems," *IEEE Trans. Power Electron.*, Vol. 29, No. 1, 191–200, 2014.
14. Trevisan, R. and A. Costanzo, "State-of-the-art of contactless energy transfer (CET) systems: Design rules and applications," *Wireless Power Transfer*, Vol. 1, No. 1, 10–20, 2014.
15. Steigerwald, R. L., "A comparison of half-bridge resonant converter topologies," *IEEE Trans. Power Electron.*, Vol. 3, No. 2, 174–182, 1988.
16. Cheng, B. and L. Z. He, "High-order network based general modeling method for improved transfer performance of the WPT system," *IEEE Trans. Power Electron.*, Vol. 36, No. 11, 12375, 2021.